MATERIALS SCIENCE

Anisotropic, lightweight, strong, and super thermally insulating nanowood with naturally aligned nanocellulose

Tian Li,[1]* Jianwei Song,[1]* Xinpeng Zhao,[2]* Zhi Yang,[3]* Glenn Pastel,[1] Shaomao Xu,[1] Chao Jia,[1] Jiaqi Dai,[1] Chaoji Chen,[1] Amy Gong,[1] Feng Jiang,[1] Yonggang Yao,[1] Tianzhu Fan,[2] Bao Yang,[3] Lars Wågberg,[4,5] Ronggui Yang,[2†] Liangbing Hu[1†]

There has been a growing interest in thermal management materials due to the prevailing energy challenges and unfulfilled needs for thermal insulation applications. We demonstrate the exceptional thermal management capabilities of a large-scale, hierarchal alignment of cellulose nanofibrils directly fabricated from wood, hereafter referred to as nanowood. Nanowood exhibits anisotropic thermal properties with an extremely low thermal conductivity of 0.03 W/m·K in the transverse direction (perpendicular to the nanofibrils) and approximately two times higher thermal conductivity of 0.06 W/m·K in the axial direction due to the hierarchically aligned nanofibrils within the highly porous backbone. The anisotropy of the thermal conductivity enables efficient thermal dissipation along the axial direction, thereby preventing local overheating on the illuminated side while yielding improved thermal insulation along the backside that cannot be obtained with isotropic thermal insulators. The nanowood also shows a low emissivity of <5% over the solar spectrum with the ability to effectively reflect solar thermal energy. Moreover, the nanowood is lightweight yet strong, owing to the effective bonding between the aligned cellulose nanofibrils with a high compressive strength of 13 MPa in the axial direction and 20 MPa in the transverse direction at 75% strain, which exceeds other thermal insulation materials, such as silica and polymer aerogels, Styrofoam, and wool. The excellent thermal management, abundance, biodegradability, high mechanical strength, low mass density, and manufacturing scalability of the nanowood make this material highly attractive for practical thermal insulation applications.

INTRODUCTION

The search for high-performance, lightweight, and mechanically strong thermally insulating materials is key to energy savings for both residential and commercial buildings, which results in a lower carbon footprint, as promoted by the U.S. Department of Energy (*1*, *2*). Good thermal insulation is also highly desirable for many electrical, optical, and space applications in which heat transfer needs to be tightly regulated. Materials for thermal insulation require a complex combination of characteristics, such as low thermal energy absorbance/emissivity, good mechanical strength, and low mass density, as well as biodegradability and cost-effectiveness (*2*–*4*). Current thermally insulating materials are typically isotropic, which is not ideal for effective thermal management. In addition, the development of isotropic thermal insulation materials has reached a plateau where further reduction of thermal conductivity leads to undesirable compromises in mechanical strength, manufacturing complexity, and performance nonstability (*5*–*8*). Typical thermally insulating materials, including wool, Styrofoam, and wood cork, often exhibit a thermal conductivity close to air (~0.03 W/m·K) (*3*, *6*, *9*, *10*), which is isotropic in nature. A low k of ~0.02 W/m·K has been obtained with silica aerogels. However, silica aerogels are brittle and difficult to prepare in large sizes.

The development of an anisotropic thermal management material has prompted substantial interest (*6*, *11*–*15*). There are significant advances in multilayer materials (superlattice) and nanomaterials with anisotropic thermal conductivities (*6*, *8*, *14*–*22*). The redirection of thermal energy in anisotropic thermal insulators can help (i) prevent heat localization and (ii) reduce heat flow in the direction of lower thermal conductivity, therefore resulting in improved thermal insulation that could not be achieved by isotropic materials. However, these types of anisotropic materials usually require complex designs and energy-consuming manufacturing processes, which thus prohibit their widespread application toward large-scale systems.

Nanocellulose is an earth-abundant biomass resource that exhibits great potential for generating sustainable products that have low environmental, human health, and safety risks (*23*–*32*). There is a substantial interest in the continuous development of value-added nanocellulose-based products that can displace their existing counterparts, such as paper-based devices and flexible light management coatings (*23*, *33*–*35*). However, the generation of nanocellulose-based products, such as cellulose foam based on a "bottom-up" approach, involves a series of mechanical and chemical processes, as well as subsequent reassembling of the cellulose nanofibrils (*36*). In addition, current techniques to reassemble cellulose nanofibrils often result in fibrils with a random orientation (*23*, *30*, *37*–*39*). The resulting products often exhibit poor mechanical properties, which have prohibited their application as insulating materials for large-scale applications in building applications and the aerospace sector. For example, Bergström *et al.* (*6*) demonstrated the first anisotropic nanocomposite super thermal insulator by freeze-drying. However, further improvement in mechanical strength and fabrication process is necessary for large-scale and realistic applications (<200 kPa in axial direction and <50 kPa in transverse direction when under 90% strain).

[1]Department of Materials Science and Engineering, University of Maryland, College Park, MD 20742, USA. [2]Department of Mechanical Engineering, University of Colorado, Boulder, CO 80309, USA. [3]Department of Mechanical Engineering, University of Maryland, College Park, MD 20742, USA. [4]Department of Fibre and Polymer Technology, School of Chemical Science and Engineering, KTH Royal Institute of Technology, Stockholm, Sweden. [5]Wallenberg Wood Science Centre, School of Chemical Science and Engineering, KTH Royal Institute of Technology, Stockholm, Sweden.
*These authors contributed equally to this work.
†Corresponding author. Email: binghu@umd.edu (L.H.); ronggui.yang@colorado.edu (R.Y.)

RESULTS

Here, we develop a simple yet effective "top-down" approach for the preparation of an anisotropic, thermally insulating bulk material by a direct chemical treatment of natural wood, which is referred as "nanowood." Inheriting the arrangement in natural wood, the nanowood is made of aligned cellulose nanofibrils, which results in anisotropic thermal conductivities, with an extremely low value of ~0.03 W/m·K in the transverse direction (perpendicular to the cellulose nanofibril alignment) and ~0.06 W/m·K along the cellulose alignment direction. This anisotropy can allow heat to spread along the nanofibril direction, which prevents local failure due to accumulated thermal energy (*11*) and reduces the heat flow in the transverse direction. The aligned cellulose nanofibrils also result in a high mechanical strength of ~13 MPa, much stronger than that of other low thermal conductivity materials such as Styrofoam, cellulose foams, and silica aerogel (*40*, *41*). We also found that the nanowood exhibits a uniquely low emissivity, making it highly efficient to block thermal radiation from the Sun.

As illustrated in Fig. 1A, when heated by a radiative heating source (Fig. 1A), the layered structure of aligned cellulose nanofibrils effectively reflects the incoming radiative energy while redirecting the absorbed heat in the planar direction. Figure 1B shows a large piece of the nanowood with a mass density of 0.130 g/cm^3. The naturally aligned wood channels (vessels and fibril tracheid lumens) facilitate effective lignin extraction while largely preserving the original micro/nanostructure. The length of the as-shown piece is around 15 cm, which demonstrates the scalability of our top-down nanowood fabrication process.

DISCUSSIONS

Mesoporous structure of the nanowood

The three major components of wood cell walls, paracrystalline cellulose fibril aggregates, amorphous heteropolysaccharide hemicellulose, and polyphenolpropane-based branched lignin, intertwine with each other to form a strong and functional vascular structure to transport water, ions, and nutrients from the roots to the leaves during photosynthesis (*42*–*44*). The nanowood is directly fabricated from natural American basswood. Note that we use American basswood as a demonstration, and that other wood species can also be used. The sample was cut along the growth direction (fig. S1). The original wood piece was treated with a mixture of NaOH and Na_2SO_3 heated to boiling temperatures, followed by subsequent treatment with H_2O_2 to remove the lignin and most of the hemicellulose from the natural wood (fig. S2) (*45*, *46*). The wood microstructure and the hierarchal alignment are well-preserved during this process, and the sample is subsequently freeze-dried (fig. S3) (*47*) to preserve the nanoporous structure of the delignified wood. The weight loss and lignin content change for a 12 mm × 30 mm × 120 mm sample during the chemical process are also shown in fig. S2. The resulting nanowood is composed of mainly

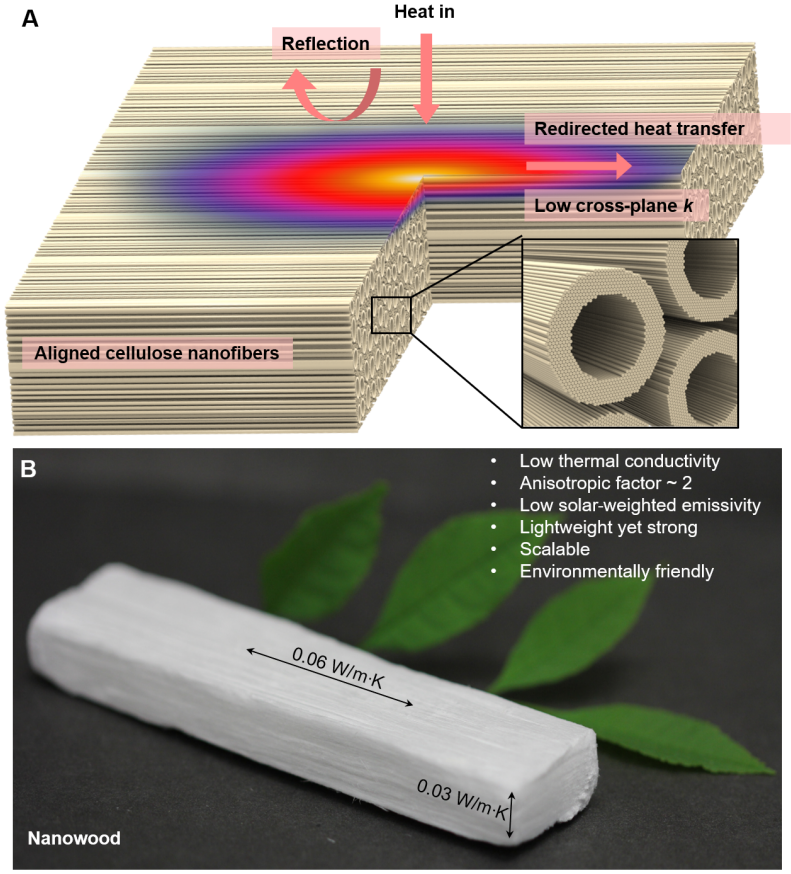

Fig. 1. Completely derived from natural wood, nanowood with hierarchically aligned cellulose nanofibrils can be used as an anisotropic super thermal insulator. (**A**) Schematics of the thermally insulating properties of the nanowood. (**B**) Digital photograph of the nanowood and the corresponding properties beneficial for building insulation applications.

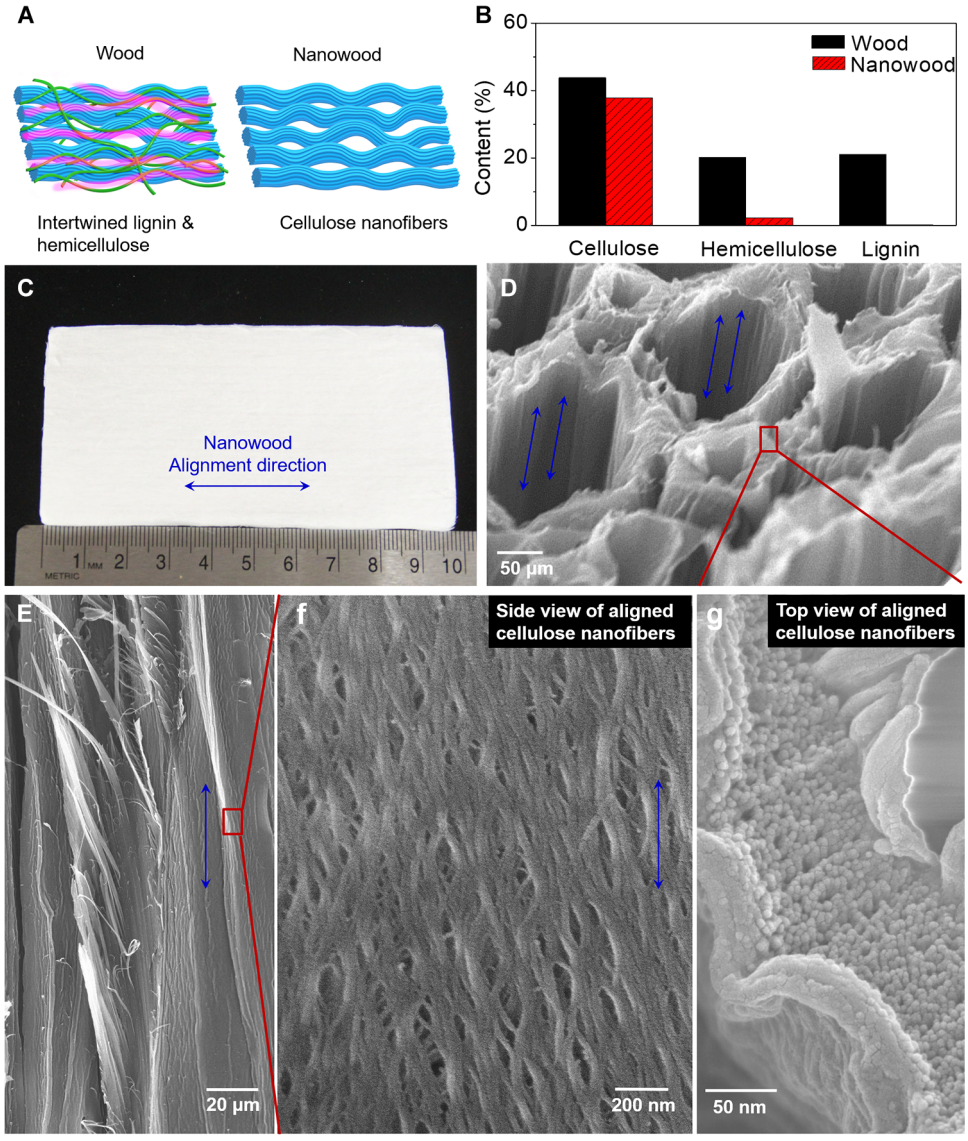

Fig. 2. Structural characterization of nanowood. (**A**) Schematics of the aligned cellulose nanofibrils in the nanowood before and after which the intermixed amorphous lignin and hemicellulose have been removed. (**B**) Concentration of lignin, hemicellulose, and cellulose in the natural wood and nanowood. (**C**) Photograph of a nanowood specimen that exhibits pure bight color and an aligned texture. (**D**) Nanowood exhibits a large porosity, a hierarchical structural alignment of fibril aggregates, and a maintained alignment of the fibril aggregates. (**E**) Side-view SEM image of the microsized porous and aligned channels inside the nanowood. (**F**) SEM image of the porous channel walls that composed of aligned nanofibrils. (**G**) Top-view SEM image of the nanowood channels with separated nanofibrils ends.

cellulose nanofibrils in the form of fibril aggregates. The effectiveness of lignin and hemicellulose removal is also demonstrated by high brightness of the fabricated nanowood (Figs. 1 and 2C, and figs. S1 to S3 and S7).

Figure 2A shows schematics of natural wood and nanowood samples. In the original natural wood specimens, amorphous lignin and hemicellulose are intertwined in between the cellulose nanofibrils (*42*–*44*). Although lignin and hemicellulose are largely removed in the nanowood (Fig. 2, A and B), the resulting structure has increased porosity and better nanofibril alignment, owing to the removal of nonalignment lignin and potential self-alignment process in the wet state. This is also in accordance with the earlier models showing how the cellulose, lignin, and hemicellulose are arranged in the fibril wall (*48*, *49*). Wood cell walls are originally composed of primary and secondary cell walls, with the latter being further divided into three layers, namely, S1, S2, and S3 (*50*). The cells are bonded with each other through a middle lamella. Among the cell wall layers, the middle S2 layer in the secondary cell wall is the thickest and is composed of parallel cellulose nanofibril aggregates aligned in a small angle difference with the length axis. The fibril angle of the S2 layer varies about 10° to 15° and can help define the alignment of the cell wall (*43*). After chemical purification, the cellulose nanofibril aggregates in the cell wall layer can be directly observed in the fibril cross section with the aid of scanning electron microscopy (SEM) (Fig. 2, D and G). In these images, it is obvious that the fibril walls are isolated from each other due to the removal of the main part of the lignin-rich middle lamella and the lignin in the primary and secondary cell wall, as shown when comparing the native wood structure with SEM in figs. S4 and S5.

The partially isolated fibrils help further reduce the transverse thermal conductivity. Because of the natural alignment of the fibrils in the wood, the individual cellulose nanofibrils that constitute the cell walls are packed and aligned parallel to each other, leading to the hierarchical alignment in the nanowood. Each fibril aggregate is composed of aligned crystalline cellulose nanofibrils with high aspect ratios (a diameter of ~30 nm and a length of approximately >1 μm) that are packed with several tens of glucan chains in a crystalline order and held together by intermolecular hydrogen bonds and van der Waals forces (*51*). The molecular alignment of the cellulose chains can be displayed by small-angle x-ray scattering characterization (fig. S6). Lignin and hemicellulose exhibit an amorphous structure, but the hemicellulose might have an alignment along the fibrils. However, the quantification of this is very limited, at least to the knowledge of the authors. The removal of lignin and hemicellulose also increases the porosity of the fibril wall structure (*49*), provided that the delignified fibrils are dried carefully to avoid a collapse of the fibril wall and to separate the fibril aggregates from each other. In addition, the effective extraction of lignin and hemicellulose naturally lowers the density of the nanowood (0.13 g/cm^3) (fig. S1).

Anisotropic thermal conduction of the nanowood

The nanowood has four key characteristics desirable for superior thermal insulation. First, from an estimation of the resulting mass density and the density of the dry cell walls, the porosity of the nanowood increases to ~91% [the density of dry cell wall of basswood is 1.491 g/cm^3 (*52*)], which is much larger than that of the original basswood (around 60%). The large porosity results in a much smaller thermal conductivity (theoretical thermal conductivity evaluation in the Supplementary Materials). Second, the removal of intermixed lignin and hemicellulose largely reduces the linkage among cellulose fibrils and the fibril aggregates within the fibril wall, leading to a much weaker interaction between fibrils and reducing the thermal conductivity in the transverse direction. Third, the aligned, high-aspect-ratio nanofibril aggregates result in anisotropic heat flow along the direction of the nanofibril alignment. Finally, most of the void channels (fibrils and vessel elements) in the nanowood are between 10 to 100 μm in diameter, whereas the individual cellulose fibrils in the cell wall fibril aggregates exhibit an interfibril aggregate spacing in the nanometer range. When the interspacing is smaller than the mean free path of air, thermal conduction through air will be impeded. However, in the mesoporous nanowood, the microsized pores dominate, and the effect of the nanosized pores on further reducing thermal conductivity is not appreciable. Further analysis of the effect of microsized and nanosized pores on the thermal conductivity of the delignified wood in both the axial and transverse directions can be found in discussion S3.

Figure 3 (A and B) shows the infrared images of anisotropic heat transfer processes in samples when irradiated by an incoming laser at the 820-nm radiation wavelength with an 0.95 W/mm^2 intensity and a spot size of 0.5 mm. For the nanowood sample cut across the growth direction, thermal energy is conducted mostly in parallel with the wood channels and remains confined in the transverse direction.

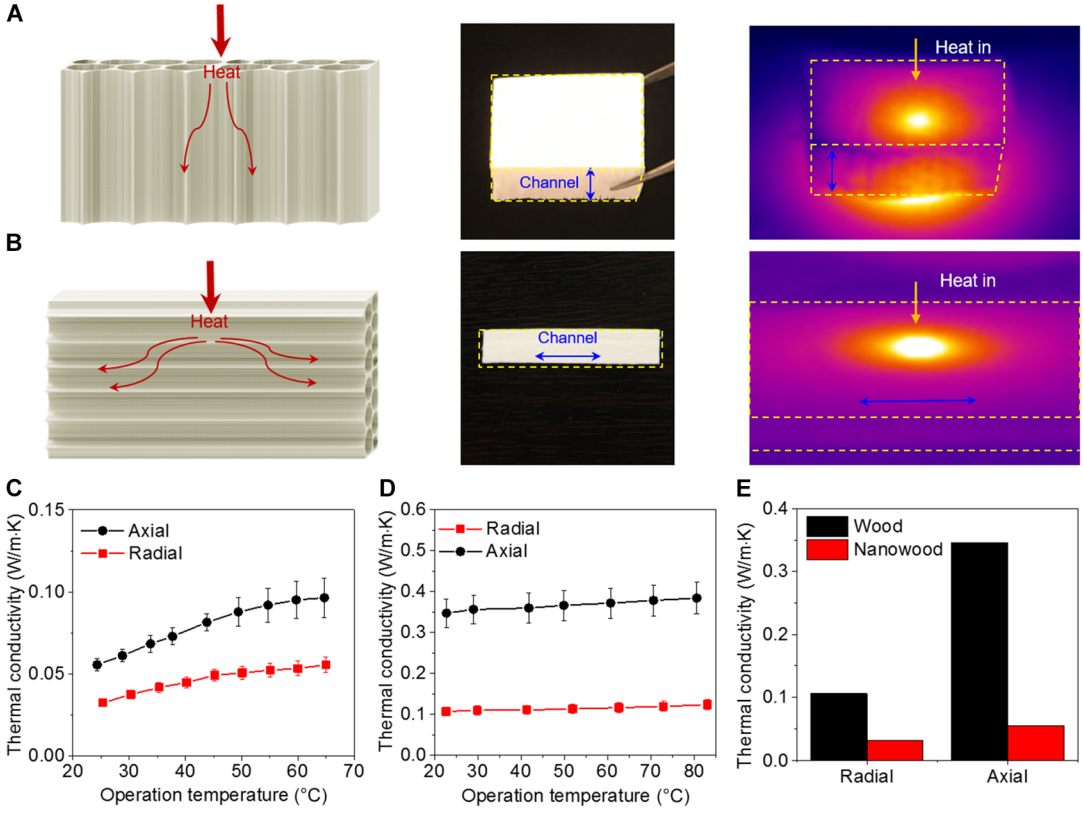

Fig. 3. Transverse and axial heat transport in nanowood. (**A**) Schematic representation of heat conduction along the wood cell walls as axial heat transfer, whereas (**B**) heat conduction across the cell walls and hollow channels (that is, the lumen and the nanosized pores inside the fibril walls) is referred to as transverse heat transfer. (**C**) Measured thermal conductivity of the nanowood from room temperature to 65°C. (**D**) Measured thermal conductivity of the original wood from room temperature to 80°C. (**E**) Comparison of the thermal conductivity of the natural wood and nanowood at room temperature.

For the nanowood sample cut along the wood growth direction, the temperature gradient profile is an elliptical shape due to the anisotropy of the thermal conductivity in the transverse and axial directions.

The thermal conductivity in the radial direction is 0.032 ± 0.002 W/m·K at 25.3°C and 0.056 ± 0.004 W/m·K at 24.3°C in the axial direction (Fig. 3C). In comparison, the natural American basswood exhibits a thermal conductivity of 0.107 ± 0.011 W/m·K in the radial direction and 0.347 ± 0.035 W/m·K in the axial direction at 22.7°C (Fig. 3D). The thermal conductivity in the natural wood stays almost constant from room temperature to 80°C. However, for the nanowood, the thermal conductivity in the transverse direction slowly rises from 0.03 to 0.055 W/m·K at higher operating temperatures, whereas in the axial direction, the value slowly changes from 0.056 to 0.10 W/m·K.

Mechanical and optical properties of the nanowood

We compared the thermal conductivity of our nanowood (in the transverse direction) and other typical thermal insulation materials, such as Styrofoam, expanded polystyrene (EPS), wool, and wood (Fig. 4A). The nanowood exhibits a lower thermal conductivity compared with most commercially available thermally insulating materials (*53*, *54*). Figure 4B summarizes the mechanical properties, including the compressive stress of existing thermally insulating materials with a thermal conductivity smaller than 0.05 W/m·K. The performance of natural wood is also added for comparison (*55*). Compressive strength has been tested along the transverse and axial directions. Mechanical tests along the transverse direction exhibit an exponentially increasing stress (fig. S8) upon compression due to densification (shown in Fig. 4B, inset). The maximum stress for compression along the axial direction is approaching 13 MPa (fig. S8). To the best of our knowledge, the strength of our nanowood represents the highest value among available super insulating materials (*6*, *40*, *41*, *56*, *57*). The building blocks of our nanowood are composed of long and aligned fibril aggregates with large surface-to-volume ratios and high aspect ratios. Because the chemical treatment of the nanowood removes almost all lignin and most of the hemicellulose, the fibril walls are more porous, and there are more spaces between the fibrils. This results in lower compression strength of the nanowood compared with the wood in the thickness direction of the fibrils. This also improves the flexibility of the samples, as demonstrated in Fig. 4C. However, because of the maintained orientation of the fibrils in the fibril wall (that is, in a twist along the fibril axis), the delignified samples have a significant strength both in the thickness direction of the fibrils but more significantly so in the length direction of the fibrils, as the mechanical properties of the fibrils are maintained because of the preservation of the orientation of the crystalline structure of the cellulose molecules, which is the load-bearing element of the fibril wall. The properties in tension and compression are thus naturally affected in a different way due to the

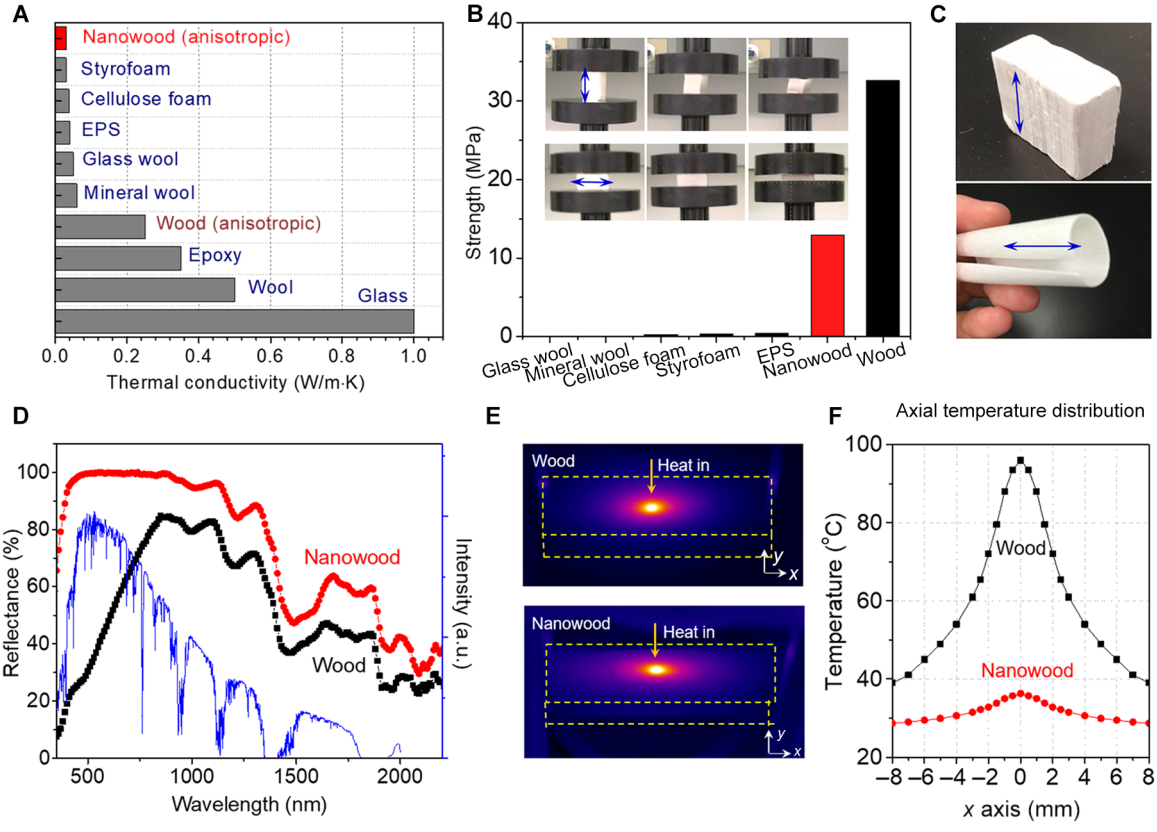

Fig. 4. Characterization of nanowood. (**A**) Thermal conductivity comparison among existing thermally insulating materials. The nanowood exhibits a very low transverse thermal conductivity along with high anisotropy. (**B**) Mechanical properties of the nanowood in comparison to other materials with a thermal conductivity smaller than 0.05 W/m·K, as well as natural basswood. (**C**) Photographs of a bulk piece of a nanowood and a thin and rollable nanowood. The arrows indicate the alignment direction. (**D**) Reflectance of the nanowood. The nanowood exhibits a larger reflectance covering the spectrum of solar radiation (that is, a low solar-weighted emissivity compared with wood). The blue curve is air mass 1.5 solar spectrum. a.u., arbitrary units. (**E**) Infrared image of the natural wood and nanowood when illuminated by a laser with a wavelength at 820 nm. (**F**) Temperature profile for the samples in (E).

difference in breakage mechanisms for these loading situations. More detailed discussion of the mechanical properties of the nanowood can be found in discussion S1 of the Supplementary Materials.

An ultraviolet-visible test (LAMBDA 35, PerkinElmer) for a 3-mm-thick sample was carried out to evaluate the emissivity of the nanowood. The sample exhibits an average of ~95% reflection, covering from 400- to 1100-nm wavelength range (Fig. 4D). The transmittance is below the basic noise level (<0.1%). The emissivity (emissivity ≈ absorptivity; gray surface approximation) is calculated to be ~5%, which indicates an effective reflection of thermal energy from the radiative heat source (Newport Standard Solar Simulator). For comparison, natural wood absorbs an average of 50% of the light in the visible light spectrum. This unique broadband omnidirectional reflectance of the bright nanowood results from the dense nanosized scattering centers on its surface (*30*, *31*). A collimated 820-nm heat source with a spot size of 1 mm and an input power of 0.95 W/mm^2 was incident perpendicular to the surface of the nanowood and the natural wood specimens. As shown in Fig. 4 (E and F), the maximum temperature is 36°C with a full width at half maximum (FWHM) of 5.2 mm on the nanowood, compared with 99.4°C on the natural wood with an FWHM of 4.0 mm, owing to (i) lower absorption and (ii) better heat dissipation of the nanowood.

Thermal insulation of the nanowood in comparison with other insulators

To demonstrate the thermal management capabilities of our developed nanowood, we tested the specimens under both a conductive and a radiative heat source and compared it against other thermal insulation materials, including a silica aerogel (isotropic), Styrofoam (isotropic), and the natural American basswood (anisotropic). The experimental setup for conductive and radiative heat transfer schemes are shown in Fig. 5 (D and G, respectively). The commercial silica aerogel (www.buyaerogel.com) has a thickness of 0.7 cm, and we prepared a nanowood

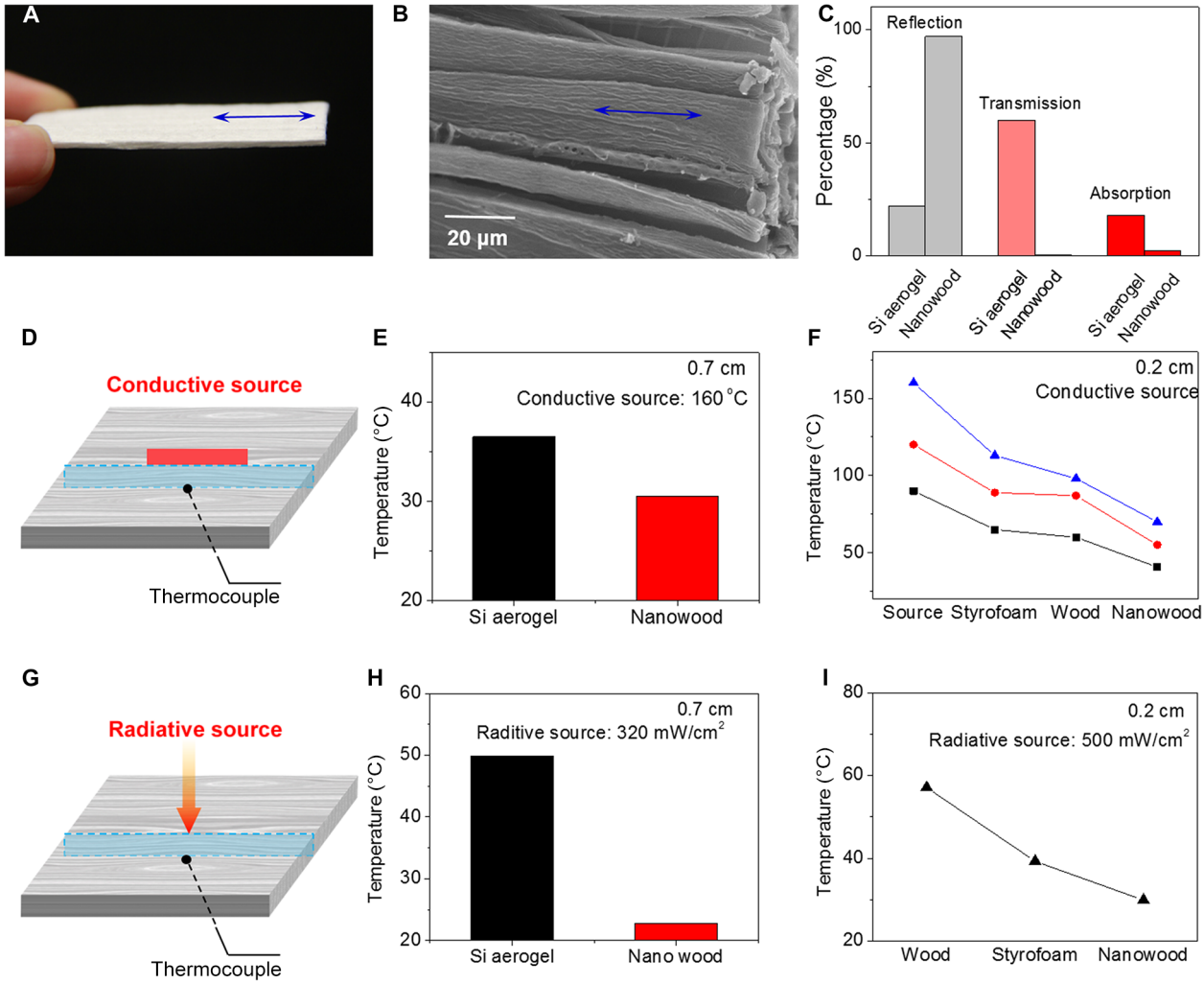

Fig. 5. Thermal insulation performance of nanowood in comparison with a silica aerogel, a Styrofoam, and a natural wood. (**A**) Photograph of a 1-mm-thick specimen of a nanowood. (**B**) SEM side view of the nanowood channels composed of aligned cellulose nanofibrils. (**C**) Optical reflection, transmission, and absorption of the silica aerogel and nanowood illuminated by the standard solar simulator. (**D**) Schematic description of the nanowood being illuminated transversely (perpendicular to the nanofibrils). (**E** and **F**) Summary of results showing the stabilized backside temperatures of the thermal insulators when the top surface is in direct contact with a conductive heat source via thermal paste. (**G**) Schematic description of the measurement setup using radiative heat sources (solar simulator). (**H** and **I**) Summary of the results showing the stabilized backside temperatures of each thermal insulator, with the top surface receiving radiative energy from the solar simulator.

block of the same size as the silica aerogel for a fair comparison. The temperature was measured with a K-type thermocouple. When heated by a conductive heat source at 160°C, it was shown that the stabilized backside temperature of silica aerogel is 36.5°C, whereas that of the nanowood is 30.5°C (Fig. 5E). We then compared the insulating performance of the delignified wood sample against Styrofoam and natural wood (Fig. 5F). Three different temperatures were applied, and the results show that the nanowood yields the lowest backside temperature, owing to the low thermal conductivity in the transverse direction in combination with the preferred thermal dissipation in the axial direction due to its anisotropy. Furthermore, the insulating performance of the different materials was evaluated under a radiative heat source. When exposed to the solar spectrum, the silica aerogel absorbs ~20% and transmits ~60% of the radiative heat. In comparison, ~95% of the radiative energy was reflected, whereas only ~2% was found absorbed by the nanowood, as summarized in Fig. 5C. The backside temperatures of the silica aerogel and the nanowood were 49.9° and 22.8°C, respectively, under 320 mW/cm^2 (Fig. 5H). This represents a much larger difference in the thermal insulation performance in comparison to the tests with a conduction-based heat source. The backside temperatures of the 2-mm-thick natural wood, Styrofoam, and nanowood samples under 500 mW/cm^2 were 57.1°, 39.3°, and 29.9°C, respectively (Fig. 5I). To further illustrate the effect of anisotropic heat conduction for the application of thermally insulating materials, a simulated temperature profile for isotropic cellulose foam (or Styrofoam/EPS) and the nanowood under radiative heat source is shown in fig. S11. Styrofoam exhibits an isotropic thermal conductivity of 0.03 W/m·K, similar to that of the nanowood in the transverse direction. Compared with an isotropic insulator, the prepared nanowood can redirect the incoming thermal energy along the axial direction, leading to a much lower frontside and backside temperature of the insulating material.

We also performed a materials cost analysis to fabricate the nanowood, including raw materials and processing chemicals (table S1), which can be as low as \$7.44/m^2. The nanowood can be processed into different shapes and sizes, suitable for versatile applications that require thermal insulation, ranging from steam and chemical pipes to building applications. Note that when the thickness is less than 1 mm, the nanowood slice can be rolled and folded, making it suitable for scenarios that require flexibility, such as pipelines in chemical factories and power plants. In addition, thermally insulating materials are typically composed of microsized components and glass wool, which can cause health concerns because the respirable fibrils can penetrate into the lungs of human beings and animals upon inhalation without degradation. On the other hand, cellulose is biodegradable, rendering it environmentally friendly when used as insulation. It should also be stressed that cellulose causes no autoimmune reactions when in contact with human tissue and cannot be degraded by the human body.

CONCLUSIONS

Completely derived from natural wood, we reported a thermally anisotropic nanowood made of hierarchically aligned cellulose nanofibrils. The newly developed nanowood exhibits excellent thermal insulation properties. Instead of using complex fabrication processes for a nanoscale anisotropic thermal insulator, such as superlattices or reconstructed layered low-dimensional materials, the nanowood can be fabricated by a scalable top-down approach via simple chemical treatments. As a proof of concept for scalability, we have demonstrated pieces of the nanowood with length larger than 15 cm and thickness larger than 2 cm. The nanowood exhibits unique anisotropic thermal properties with a low transverse thermal conductivity of 0.03 W/m·K with an anisotropy of 2 (higher axial thermal conductivity of ~0.06 W/m·K). The nanowood also has the following unique properties: (i) a high mechanical strength of 13 MPa, owing to the crystalline ordering of the glucan chains of the cellulose fibrils, which is ~50 times higher than cellulose foam and >30 times higher than the commercially used strongest thermal insulation materials; (ii) low mass density; (iii) low emissivity from 400 to 1100 nm; and (iv) abundant, sustainable, and potentially low cost. The newly developed nanowood as a super thermal insulator with a low thermal conductivity can potentially find applications in energy-efficient buildings, thermal insulation for space applications, and electrical devices insulation.

METHODS

Mechanical test

The compressive tests of the specimen were performed using a Tinius Olsen H25KT testing machine. Two samples were compressed along the transverse and axial directions, respectively. Specimens of 5-mm width were tested at a gauge length of 25 mm and a cross-head speed of 5 mm min^{-1}.

Direct temperature measurement under different heating sources

A conductive heat source with a contact area of 4 mm × 4 mm was used in direct contact with the thermally insulating materials via a conductive thermal paste. A solar simulator from Newport was used to provide radiative thermal energy that incidents perpendicular to the top surface of the insulators with an illuminating spot size of 5 mm. The surrounding temperature was 21°C during when the measurements were performed. The K-type gauge thermocouple was applied with a heat conductive thermal paste. Steady state was reached before the data were recorded.

Thermal conductivity measurement

The temperature and humidity chamber was used to store the sample for a minimum of 24 hours at 25°C and 20% humidity before measurement. In our measurement, the humidity was controlled to be 20%, while the temperature dependence of the thermal conductivity was recorded. Laser flash apparatus (LFA) is a noncontact transient method to measure thermal diffusivity of materials, which has been applied to test the vast majority of bulk materials, including organic-inorganic hybrid composites (*58*–*60*) and metal-semiconductor nanocomposites (*61*). According to Feng *et al.* (*62*) and Wiener *et al.* (*63*), LFA can be used to measure aerogels whose thermal conductivities are as low as 0.01 W/m·K. During the measurement, an instantaneous laser pulse was used to heat up one side of the sample, and the response of temperature on the other side was recorded by a detector. Here, the Netzsch LFA (LFA 457) was used for thermal diffusivity measurement. The thermal conductivity k of the sample can then be calculated by the following equation

$$k = \alpha \rho C_p \quad (1)$$

where α (mm^2/s) is the measured thermal diffusivity along a particular direction, ρ is the density, and C_p is the heat capacity. Differential

scanning calorimetry (DSC) method was used to determine the heat capacity. Using Netzsch DSC 204 F1 Phoenix, the heat capacities were acquired through three steps: (i) determining the heat flow rate of zero line with two empty crucibles, with one being the reference and the other being the sample; (ii) measuring the reference samples with known heat capacity in sample crucibles; and (iii) measuring the samples. In our measurements, the sapphire was used as a reference material because its heat capacity is well known to range from 70 to 2500 K. Six pieces of nanowood samples (same densities) were measured for a temperature range of 22° to 65°C, with three in the transverse direction and another three in the axial direction. The error bar was generated on the basis of sample variation and equipment error. Using the thermal diffusivity and heat capacity data obtained above, Fig. 3C shows the thermal conductivity of nanowood samples calculated using Eq. 1. The error bar for the thermal conductivity was calculated on the basis of the measured data and the error bar of heat capacity, diffusivity, and mass density after testing six different samples (0.13 ± 0.03 g/cm^3).

SUPPLEMENTARY MATERIALS

Supplementary material for this article is available at http://advances.sciencemag.org/cgi/content/full/4/3/eaar3724/DC1

fig. S1. Nanowood is composed of hierarchical aligned nanofibrillar cellulose arrays derived from natural wood.
fig. S2. The lignin content and appearance between chemical processes.
fig. S3. Nanowood drying process.
fig. S4. SEM images of natural wood.
fig. S5. SEM images of nanowood.
fig. S6. Molecular level alignment in the hierarchal alignment of nanowood.
fig. S7. Nanowood samples can be fabricated within a wide size distribution.
fig. S8. Compressive stress test of nanowood along the axial and radial direction.
fig. S9. Tensile strength of the nanowood and original wood.
fig. S10. Comparison between commercially available silica aerogel and nanowood.
fig. S11. Temperature plots of isotropic and anisotropic thermal insulators from a point heat source.
fig. S12. The two levels of porosity (microsized and nanosized pores) in nanowood.
fig. S13. Thermogravimetric analysis.
fig. S14. Digital images of the delignified wood piece after >1 year under ambient environment.
fig. S15. Air permeability test of nanowood.
fig. S16. Industry compatible wood board cutting method.
fig. S17. Nanowood is composed of aligned cellulose nanofibers with mesoporous structure.
fig. S18. Reflectance comparison between vertically cut plane and horizontally cut plane of nanowood.
fig. S19. Thermal conductivity in transverse and axial direction under humidity of 20% and 80%, respectively.
fig. S20. The tensile strength of nanowood under 20 and 80% humidity.
table S1. Materials cost for nanowood production.
table S2. Comparison between nanowood, paper, and honeycomb paper wraps.
discussion S1. Mechanical property analysis of nanowood
discussion S2. Numerical simulations of isotropic and anisotropic thermal insulators
discussion S3. Thermal conductivity estimation
discussion S4. Thermal stability of nanowood
discussion S5. Permeability of nanowood
discussion S6. Scalable manufacturing
discussion S7. Comparison with a stack of paper and honeycomb wrapping paper
discussion S8. The effect of humidity
References (*64*–*70*)

REFERENCES AND NOTES

1. U.S. Department of Energy, Buildings; https://energy.gov/eere/buildings/building-technologies-office.
2. U.S. Department of Energy, Guiding Principles for Sustainable Federal Buildings; https://energy.gov/eere/femp/guiding-principles-sustainable-federal-buildings.
3. B. P. Jelle, Traditional, state-of-the-art and future thermal building insulation materials and solutions – Properties, requirements and possibilities. *Energy Build.* **43**, 2549–2563 (2011).
4. M. S. Al-Homoud, Performance characteristics and practical applications of common building thermal insulation materials. *Build. Environ.* **40**, 353–366 (2005).
5. H. S. Kim, T. Wang, W. Liu, Z. Ren, Engineering thermal conductivity for balancing between reliability and performance of bulk thermoelectric generators. *Adv. Funct. Mater.* **26**, 3678–3686 (2016).
6. B. Wicklein, A. Kocjan, G. Salazar-Alvarez, F. Carosio, G. Camino, M. Antonietti, L. Bergström, Thermally insulating and fire-retardant lightweight anisotropic foams based on nanocellulose and graphene oxide. *Nat. Nanotechnol.* **10**, 277–283 (2015).
7. J. P. Heremans, M. S. Dresselhaus, L. E. Bell, D. T. Morelli, When thermoelectrics reached the nanoscale. *Nat. Nanotechnol.* **8**, 471–473 (2013).
8. Y. Hu, L. Zeng, A. J. Minnich, M. S. Dresselhaus, G. Chen, Spectral mapping of thermal conductivity through nanoscale ballistic transport. *Nat. Nanotechnol.* **10**, 701–706 (2015).
9. A. M. Papadopoulos, State of the art in thermal insulation materials and aims for future developments. *Energy Build.* **37**, 77–86 (2005).
10. D. Bozsaky, The historical development of thermal insulation materials. *Period. Polytech. Archit.* **41**, 49–56 (2010).
11. J. D. Renteria, S. Ramirez, H. Malekpour, B. Alonso, A. Centeno, A. Zurutuza, A. I. Cocemasov, D. L. Nika, A. A. Balandin, Strongly anisotropic thermal conductivity of free-standing reduced graphene oxide films annealed at high temperature. *Adv. Funct. Mater.* **25**, 4664–4672 (2015).
12. Y. Lan, Z. Ren, Thermoelectric nanocomposites for thermal energy conversion, in *Nanomaterials for Sustainable Energy*, Q. Li, Ed. (Springer, 2016).
13. S. Lee, K. Esfarjani, T. Luo, J. Zhou, Z. Tian, G. Chen, Resonant bonding leads to low lattice thermal conductivity. *Nat. Commun.* **5**, 3525 (2014).
14. T. Borca-Tasciuc, S. Vafaei, D.-A. Borca-Tasciuc, B. Q. Wei, R. Vajtai, P. M. Ajayan, Anisotropic thermal diffusivity of aligned multiwall carbon nanotube arrays. *J. Appl. Phys.* **98**, 054309 (2005).
15. L. Guo, J. Wang, Z. Lin, S. Gacek, X. Wang, Anisotropic thermal transport in highly ordered TiO_2 nanotube arrays. *J. Appl. Phys.* **106**, 123526 (2009).
16. C. Wan, X. Gu, F. Dang, T. Itoh, Y. Wang, H. Sasaki, M. Kondo, K. Koga, K. Yabuki, G. J. Snyder, R. Yang, K. Koumoto, Flexible n-type thermoelectric materials by organic intercalation of layered transition metal dichalcogenide TiS_2. *Nat. Mater.* **14**, 622–627 (2015).
17. J. Liu, B. Yoon, E. Kuhlmann, M. Tian, J. Zhu, S. M. George, Y.-C. Lee, R. Yang, Ultralow thermal conductivity of atomic/molecular layer-deposited hybrid organic–inorganic zincone thin films. *Nano Lett.* **13**, 5594–5599 (2013).
18. C. Chiritescu, D. G. Cahill, N. Nguyen, D. Johnson, A. Bodapati, P. Keblinski, P. Zschack, Ultralow thermal conductivity in disordered, layered WSe_2 crystals. *Science* **315**, 351–353 (2007).
19. M. D. Losego, I. P. Blitz, R. A. Vaia, D. G. Cahill, P. V. Braun, Ultralow thermal conductivity in organoclay nanolaminates synthesized via simple self-assembly. *Nano Lett.* **13**, 2215–2219 (2013).
20. E. S. Toberer, L. L. Baranowski, C. Dames, Advances in thermal conductivity. *Annu. Rev. Mater. Res.* **42**, 179–209 (2012).
21. S. Volz, *Thermal Nanosystems and Nanomaterials* (Springer, 2009).
22. C. H. Li, G. P. Peterson, Dual role of nanoparticles in the thermal conductivity enhancement of nanoparticle suspensions, in *ASME 2005 International Mechanical Engineering Congress and Exposition (IMECE2005)*, Orlando, FL, 5 to 11 November 2005.
23. Y. H. Jung, T.-H. Chang, H. Zhang, C. Yao, Q. Zheng, V. W. Yang, H. Mi, M. Kim, S. J. Cho, D.-W. Park, H. Jiang, J. Lee, Y. Qiu, W. Zhou, Z. Cai, S. Gong, Z. Ma, High-performance green flexible electronics based on biodegradable cellulose nanofibril paper. *Nat. Commun.* **6**, 7170 (2015).
24. I. A. Sacui, R. C. Nieuwendaal, D. J. Burnett, S. J. Stranick, M. Jorfi, C. Weder, E. J. Foster, R. T. Olsson, J. W. Gilman, Comparison of the properties of cellulose nanocrystals and cellulose nanofibrils isolated from bacteria, tunicate, and wood processed using acid, enzymatic, mechanical, and oxidative methods. *ACS Appl. Mater. Interfaces* **6**, 6127–6138 (2014).
25. J. Majoinen, J. Hassinen, J. S. Haataja, H. T. Rekola, E. Kontturi, M. A. Kostiainen, R. H. A. Ras, P. Törmä, O. Ikkala, Chiral plasmonics using twisting along cellulose nanocrystals as a template for gold nanoparticles. *Adv. Mater.* **28**, 5262–5267 (2016).
26. L. R. Arcot, K. M. A. Uddin, X. Chen, X. Wenchao, K. Xianming, L. S. Johansson, R. H. A. Ras, O. J. Rojas, Paper-based plasmon-enhanced protein sensing by controlled nucleation of silver nanoparticles on cellulose. *Cellulose* **22**, 4027–4034 (2015).
27. J. Y. Zhu, R. Sabo, X. Luo, Integrated production of nano-fibrillated cellulose and cellulosic biofuel (ethanol) by enzymatic fractionation of wood fibers. *Green Chem.* **13**, 1339–1344 (2011).
28. Y. Habibi, L. A. Lucia, O. J. Rojas, Cellulose nanocrystals: Chemistry, self-assembly, and applications. *Chem. Rev.* **110**, 3479–3500 (2010).
29. J. Simonsen, Utilizing straw as a filler in thermoplastic building materials. *Constr. Build. Mater.* **10**, 435–440 (1996).

30. L. Hu, G. Zheng, J. Yao, N. Liu, B. Weil, M. Eskilsson, E. Karabulut, Z. Ruan, S. Fan, J. T. Bloking, M. D. McGehee, L. Wågberg, Y. Cui, Transparent and conductive paper from nanocellulose fibers. *Energy Environ. Sci.* **6**, 513–518 (2013).
31. Z.-Y. Wu, C. Li, H.-W. Liang, J.-F. Chen, S.-H. Yu, Ultralight, flexible, and fire-resistant carbon nanofiber aerogels from bacterial cellulose. *Angew. Chem. Int. Ed. Engl.* **125**, 2997–3001 (2013).
32. L.-F. Chen, Z.-H. Huang, H.-W. Liang, W.-T. Yao, Z.-Y. Yu, S.-H. Yu, Flexible all-solid-state high-power supercapacitor fabricated with nitrogen-doped carbon nanofiber electrode material derived from bacterial cellulose. *Energy Environ. Sci.* **6**, 3331–3338 (2013).
33. H. Zhu, W. Luo, P. N. Ciesielski, Z. Fang, J. Y. Zhu, G. Henriksson, M. E. Himmel, L. Hu, Wood-derived materials for green electronics, biological devices, and energy applications. *Chem. Rev.* **116**, 9305–9374 (2016).
34. K. M. O. Håkansson, A. B. Fall, F. Lundell, S. Yu, C. Krywka, S. V. Roth, G. Santoro, M. Kvick, L. P. Wittberg, L. Wågberg, L. D. Söderberg, Hydrodynamic alignment and assembly of nanofibrils resulting in strong cellulose filaments. *Nat. Commun.* **5**, 4018 (2014).
35. Y. Yao, J. Tao, J. Zou, B. Zhang, T. Li, J. Dai, M. Zhu, S. Wang, K. K. Fu, D. Henderson, E. Hitz, J. Peng, L. Hu, Light management in plastic–paper hybrid substrate towards high-performance optoelectronics. *Energy Environ. Sci.* **9**, 2278–2285 (2016).
36. A. J. Svagan, M. A. S. A. Samir, L. A. Berglund, Biomimetic foams of high mechanical performance based on nanostructured cell walls reinforced by native cellulose nanofibrils. *Adv. Mater.* **20**, 1263–1269 (2008).
37. Z. M. Ali, L. J. Gibson, The structure and mechanics of nanofibrillar cellulose foams. *Soft Matter* **9**, 1580–1588 (2013).
38. Z. Fang, H. Zhu, W. Bao, C. Preston, Z. Liu, J. Dai, Y. Li, L. Hu, Highly transparent paper with tunable haze for green electronics. *Energy Environ. Sci.* **7**, 3313–3319 (2014).
39. Y. Qing, R. Sabo, J. Y. Zhu, U. Agarwal, Z. Cai, Y. Wu, A comparative study of cellulose nanofibrils disintegrated via multiple processing approaches. *Carbohydr. Polym.* **97**, 226–234 (2013).
40. V. Vaou, D. Panias, Thermal insulating foamy geopolymers from perlite. *Miner. Eng.* **23**, 1146–1151 (2010).
41. I. Gnip, S. Vaitkus, V. Keršulis, S. Vėjelis, Predicting the deformability of mineral wool slabs under constant compressive stress. *Constr. Build. Mater.* **23**, 1928–1934 (2009).
42. E. Sjostrom, *Wood Chemistry* (Elsevier, ed. 2, 2013).
43. R. H. White, Effect of lignin content and extractives on the higher heating value of wood. *Wood Fiber Sci.* **19**, 446–452 (1987).
44. R. M. Rowell, *Handbook of Wood Chemistry and Wood Composites* (CRC Press, ed. 2, 2012).
45. M. Zhu, J. Song, T. Li, A. Gong, Y. Wang, J. Dai, Y. Yao, W. Luo, D. Henderson, L. Hu, Highly anisotropic, highly transparent wood composites. *Adv. Mater.* **28**, 5181–5187 (2016).
46. T. Li, M. Zhu, Z. Yang, J. Song, J. Dai, Y. Yao, W. Luo, G. Pastel, B. Yang, L. Hu, Wood composite as an energy efficient building material: Guided sunlight transmittance and effective thermal insulation. *Adv. Energy Mater.* **6**, 1601122 (2016).
47. S. Deville, E. Saiz, R. K. Nalla, A. P. Tomsia, Freezing as a path to build complex composites. *Science* **311**, 515–518 (2006).
48. A. J. Kerr, D. A. I. Goring, The ultrastructural arrangement of the wood cell wall. *Cellul. Chem. Technol.* **9**, 563–573 (1975).
49. J. E. Stone, A. M. Scallan, Effect of component removal upon the porous structure of the cell wall of wood. *J. Polym. Sci. Pol. Sym.* **11**, 13–25 (1965).
50. T. A. Tabet, F. A. Aziz, Cellulose microfibril angle in wood and its dynamic mechanical significance, in *Cellulose - Fundamental Aspects*, T. van de Ven, L. Godbout, Eds. (InTech, 2013).
51. E.-l. Hult, "CP/MAS 13C-NMR spectroscopy applied to structure and interaction studies on wood an pulp fibers," thesis, KTH Royal Institute of Technology, Stockholm, Sweden (2001).
52. R. M. Kellogg, F. F. Wangaard, Variation in the cell-wall density of wood. *Wood Fiber Sci.* **1**, 180–204 (2007).
53. Thermal conductivity of common materials and gases, www.engineeringtoolbox.com/thermal-conductivity-d_429.html.
54. Thermal insulation materials, technical characteristics and selection criteria, www.fao.org/docrep/006/y5013e/y5013e08.htm.
55. D. W. Green, J. E. Winandy, D. E. Kretschmann, Mechanical properties of wood, in *Wood Handbook: Wood as an Engineering Material* (U.S. Department of Agriculture, Forest Service, Forest Products Laboratory, 1999).
56. Eco-Panels vs. Traditional SIPs, www.eco-panels.com/about-epanels-vs-tradsips.html.
57. Ecology benchmarking extended with GLAPOR cellular glass (2015); https://belglas.com/2015/11/17/ecology-benchmarking-extended-with-glapor-cellular-glass/).
58. X. Huang, M. Roushan, T. J. Emge, W. Bi, S. Thiagarajan, J.-H. Cheng, R. Yang, J. Li, Flexible hybrid semiconductors with low thermal conductivity: The role of organic diamines. *Angew. Chem. Int. Ed. Engl.* **48**, 7871–7874 (2009).
59. M. Wu, J. Rhee, T. J. Emge, H. Yao, J.-H. Cheng, S. Thiagarajan, M. Croft, R. Yang, J. Li, A low band gap iron sulfide hybrid semiconductor with unique 2D $[Fe_{16}S_{20}]^{8-}$ layer and reduced thermal conductivity. *Chem. Commun.* **46**, 1649–1651 (2010).
60. Y.-C. Chen, H. Yao, S. Thiagarajan, M. Wu, T. J. Emge, R. Yang, S. Yu, J. Li, Layered hybrid selenoantimonates with reduced thermal conductivity. *Z. Anorg. Allg. Chem.* **638**, 2604–2609 (2012).
61. T. Shuvra Basu, R. Yang, S. J. Thiagarajan, S. Ghosh, S. Gierlotka, M. Ray, Remarkable thermal conductivity reduction in metal-semiconductor nanocomposites. *Appl. Phys. Lett.* **103**, 083115 (2013).
62. J. Feng, J. Feng, C. Zhang, Thermal conductivity of low density carbon aerogels. *J. Porous Mater.* **19**, 551–556 (2012).
63. M. Wiener, G. Reichenauer, S. Braxmeier, F. Hemberger, H.-P. Ebert, Carbon aerogel-based high-temperature thermal insulation. *Int. J. Thermophys.* **30**, 1372–1385 (2009).
64. H. Zhu, S. Zhu, Z. Jia, S. Parvinian, Y. Li, O. Vaaland, L. Hu, T. Li, Anomalous scaling law of strength and toughness of cellulose nanopaper. *Proc. Natl. Acad. Sci. U.S.A.* **112**, 8971–8976 (2015).
65. Properties of paper, www.paperonweb.com/paperpro.htm.
66. M. G. Kaganer, *Thermal Insulation in Cryogenic Engineering* (Israel Program for Scientific Translations, 1969).
67. J. Eitelberger, K. Hofstetter, Prediction of transport properties of wood below the fiber saturation point – A multiscale homogenization approach and its experimental validation: Part I: Thermal conductivity. *Compos. Sci. Technol.* **71**, 134–144 (2011).
68. B. M. Suleiman, J. Larfeldt, B. Leckner, M. Gustavsson, Thermal conductivity and diffusivity of wood. *Wood Sci. Technol.* **33**, 465–473 (1999).
69. H. Yang, R. Yan, H. Chen, D. H. Lee, C. Zheng, Characteristics of hemicellulose, cellulose and lignin pyrolysis. *Fuel* **86**, 1781–1788 (2007).
70. S. A. Lavrykov, B. V. Ramarao, Thermal properties of copy paper sheets. *Drying Technol.* **30**, 297–311 (2012).

Acknowledgments: We acknowledge the support of the Maryland NanoCenter and its AIMLab. We acknowledge the help from J.Y. Zhu at the U.S. Forest Products Laboratory on the compositional analysis of original and delignified wood. We also acknowledge the help from R. J. Bonenberger and H. Hao at University of Maryland on the mechanical tests. **Funding:** The authors acknowledge that they received no funding in support of this research. **Author contributions:** T.L. and L.H. conceived the idea and designed the experiments. J.S., T.L., C.J., and A.G. contributed to the sample preparation and scale-up optimization. X.Z., T.L., Z.Y., R.Y., B.Y., and T.F. conducted the thermal conductivity measurement and modeling, as well as thermal the insulation characterization. T.L., J.S., J.D., C.C., G.P., and Y.Y. were responsible for the SEM images, compositional analysis, and mechanical tests. T.L., F.J., S.X., and L.W. contributed to the discussion and the characterization of the delignified wood. **Competing interests:** L.H. and T.L. are inventors on a patent application related to this work (University of Maryland Invention Disclosure PS-2017-117, filed 09 January 2017). All other authors declare that they have no competing interests. **Data and materials availability:** All data needed to evaluate the conclusions in the paper are present in the paper and/or the Supplementary Materials. Additional data related to this paper may be requested from the authors.

Submitted 1 November 2017
Accepted 2 February 2018
Published 9 March 2018
10.1126/sciadv.aar3724

Citation: T. Li, J. Song, X. Zhao, Z. Yang, G. Pastel, S. Xu, C. Jia, J. Dai, C. Chen, A. Gong, F. Jiang, Y. Yao, T. Fan, B. Yang, L. Wågberg, R. Yang, L. Hu, Anisotropic, lightweight, strong, and super thermally insulating nanowood with naturally aligned nanocellulose. *Sci. Adv.* **4**, eaar3724 (2018).